ChemPubSoc Europe

DOI: 10.1002/chem.201903808

CHEMISTRY A European Journal Full Paper

Enzyme Models

Rational De Novo Design of a Cu Metalloenzyme for Superoxide Dismutation

Emilie Mathieu[+],[b] Audrey E. Tolbert[+],[a] Karl J. Koebke,[a] Cédric Tard,[c] Olga Iranzo,[d] James E. Penner-Hahn,[a] Clotilde Policar,*[b] and Vincent Pecoraro*[a]

Abstract: Superoxide dismutases (SODs) are highly efficient enzymes for superoxide dismutation and the first line of defense against oxidative stress. These metalloproteins contain a redox-active metal ion in their active site (Mn, Cu, Fe, Ni) with a tightly controlled reduction potential found in a close range around the optimal value of 0.36 V versus the normal hydrogen electrode (NHE). Rationally designed proteins with well-defined three-dimensional structures offer new opportunities for obtaining functional SOD mimics. Here, we explore four different copper-binding scaffolds: H_3 (His_3), H_4 (His_4), H_2DH (His_3Asp with two His and one Asp in the same plane) and H_3D (His_3Asp with three His in the same plane) by using the scaffold of the de novo protein GRα_3D. EPR and XAS analysis of the resulting copper complexes demonstrates that they are good Cu^{II}-bound structural mimics of Cu-only SODs. Furthermore, all the complexes exhibit SOD activity, though three orders of magnitude slower than the native enzyme, making them the first de novo copper SOD mimics.

Introduction

Superoxide dismutases (SODs) are highly conserved metalloenzymes that have evolved to protect organisms from oxidative stress.[1,2] Four types of SODs have been identified, but only three have been extensively studied (Table 1).[1,3] The first well-characterized class of SODs is the Fe/MnSOD, which can function with iron only, manganese only, or either metal in the case of cambialistic enzymes. These proteins have high sequence identity and the same His_3Asp metal-binding site regardless of the active metal.[4] The second is the NiSOD, which contains a His_2Cys binding site.[5] The third type of well-characterized SODs are Cu/ZnSODs. General features of Cu/ZnSODs include a Greek key β-barrel backbone, an electrostatic loop, a disulfide bond, and a conserved active site.[1–3] In its reduced state, the catalytic copper is bound by three histidines in a trigonal plane. Upon oxidation, the Cu^{II} is bound in a distorted square pyramid by an additional, bridging histidine and a water molecule. The bridging histidine also binds to the structural zinc ion, which is further coordinated by two other histidines and an aspartate.[1] Interestingly, a fourth class of SODs, that is, Cu-only SODs, has recently been described containing a single copper metal ion in the active site.[6–10] In these enzymes, the two histidines chelating the zinc ion in Cu/Zn SODs are missing, either due to substitution or deletion. Thus, the active site only contains four histidines capable of chelating copper. All four His residues coordinate Cu^{II} in a pseudo-trigonal pyramid, whereas Cu^{I} is coordinated by only three His residues in a pseudo-trigonal-planar arrangement with the fourth His at a longer distance.[6] In *C. albicans* Cu-only SOD5, the role of the zinc ion in promoting pH-independent catalysis is adopted by a glutamate residue (Glu110) that interacts through hydrogen bonding with the bridging histidine.[10]

Despite their differences in structure, active site, and metal center, all SODs catalyze superoxide dismutation at diffusion-

Table 1. Summary of SODs activities.

SOD	Activity [$M^{-1}s^{-1}$]	pH
Fe[11]	3.25×10^9	7.8
Mn[11]	3.78×10^9	7.8
Ni[12]	1.3×10^9	7.0
Cu/Zn[6]	1.2×10^9	7.0
Cu only[6]	1.8×10^9	6.0
	1.1×10^9	7.25
cyclodextran (Cu/Zn)[13]	9.90×10^7	7.8
N-term Cu/Zn model HADHDHKK[14]	2.7×10^7	7.0

[a] *A. E. Tolbert,[+] Dr. K. J. Koebke, Prof. J. E. Penner-Hahn, Prof. V. Pecoraro*
Department of Chemistry
University of Michigan
Ann Arbor, MI 48103 (USA)
E-mail: vlpec@umich.edu

[b] *Dr. E. Mathieu,[+] Prof. C. Policar*
Laboratoire des biomolécules, LBM, Département de chimie
École normale supérieure, PSL University, Sorbonne Université, CNRS
75005 Paris (France)
E-mail: clotilde.policar@ens.fr

[c] *Prof. C. Tard*
LCM, CNRS, Ecole Polytechnique, IP Paris
91128 Palaiseau (France)

[d] *Dr. O. Iranzo*
Centrale Marseille, iSm2
Aix-Marseille Université, CNRS
Marseille (France)

[+] *These authors contributed equally to this work*

limited rates between pH 4 and 10.[1] Their reduction potentials are tightly controlled and fall in a close range around the optimal value of 0.36 V versus the normal hydrogen electrode (NHE) at physiological pH, corresponding to the midpoint potential between the oxidation (−0.18 V vs. NHE) and the reduction (+0.91 V26 vs. NHE) of superoxide.[1]

Low-molecular-weight complexes mimicking SODs with a manganese, iron, or copper metal ion have been thoroughly described in the literature.[2,15–22] The challenges faced in their design include stability, flexibility to adapt the coordination of different metal redox states, and tuning the reduction potential to enable superoxide dismutation. For Cu/Zn SOD mimics, cyclodextrin[13,20] and bisdioxocyclan derivatives[23,24] are among the most efficient SOD mimics reported, with k_{cat} values only ten-fold lower than that of the native enzyme under similar conditions. Peptidic Cu/Zn SOD mimics have also been studied,[14,25–33] with the aim to reproduce the active site of the enzyme by using short sequences of amino acids (three to ten residues) that contain two to four histidine moieties. One of the most active peptidic mimics of Cu/ZnSODs was reported by Árus et al.[14] These unstructured peptide sequences contain three histidines (HADHDHKK) and bind copper in a 1:1 ratio. At pH 7.0 its k_{cat} value is 2.7 10^7 M^{-1} s^{-1}, which is only two orders of magnitude lower than that of the native Cu/Zn SOD. As many of these peptidic models are mononuclear Cu catalysts, they can provide some amount of insight into the Cu-only SOD system, but no models of Cu-only SODs have previously been described.

Widening possibilities beyond low-molecular-weight complexes, rationally designed self-assembling peptidic scaffolds with well-defined secondary and tertiary structures are tools of choice to mimic the structure and activity of an enzyme.[34–42] Only one manganese SOD mimic has been reported, which uses this type of construct with modest SOD activity (k_{cat} = 3.7 10^5 M^{-1} s^{-1} at pH 7.4).[43] By using protein redesign Benson et al. have obtained a functional iron SOD mimic by introducing a His_3 metal-binding site and a pocket for O_2 binding into *E. coli* thioredoxin (k_{cat} = 6.4 10^6 M^{-1} s^{-1} at pH 8).[44,45]

Herein, the GRα_3D de novo protein scaffold was used to design a functional mimic of Cu-only SODs. The α_3D family of proteins, originally designed by DeGrado et al., consists of seven amino acid repeats in which the first and fourth residue of each heptad is hydrophobic.[36] In solution, these hydrophobic residues collapse to form the core of an antiparallel three-helix bundle.[35,46] Metal-binding residues can then be introduced into this core to construct metalloproteins, though a loss of stability is incurred.[47–49] This scaffold has previously been used to study both electron-transfer proteins, such as cupredoxins and rubredoxins, and catalytic proteins, such as carbonic anhydrase.[47,49–52] An elongated version of this peptide, GRα_3D, was designed with an additional heptad for improved thermodynamic stability.[53] Four binding sites were introduced into the protein; H_3 (His_3), H_4 (His_4), H_2DH (His_3Asp with two His and one Asp in the same plane), and H_3D (His_3Asp with three His in the same plane) (Table 2). The stability of the apo- and Cu^{II} protein was studied by thermal denaturation and the complexes were characterized by electron paramagnetic resonance (EPR), extended X-ray absorption fine structure (EXAFS), and cyclovoltammetry (CV) experiments. Their SOD activity was assessed by the indirect assay of McCord–Fridovich.[54–56]

Results

Protein design

Four constructs were built within the GRα_3D de novo protein scaffold with varying active sites meant to recapitulate that of two different classes of SODs, the is, Cu-only SODs and Fe/MnSODs. Their sequences are listed in Table 2. Constructs with an A98C mutation were used for electrochemical experiments. The four different active sites designed within GRα_3D for this study are represented in Figure 1. GRα_3D H_3 contains three his-

Table 2. Designed protein amino acid sequences with mutations from GRα3D in bold and active site residues in blue. Electrochemical studies were performed with derivatives having a terminal Cys rather than Ala (A98C) indicated by A/C.

Peptide	Sequence
GRα_3D H_3	MGSWAEFKQRLAAIKTRLAAIK**S**R**HD**ALGGS-EAELAA**H**EKEIAAFESEIAAFESELQAYKGKG-NPEVEALRKEAAAIRDEAAAIRDE**H**QAYRLNGSG**A/C**
GRα_3D H_4	MGSWAEFKQRLAAIKTRLAAIK**S**R**HD**ALGGS-EAE**H**AA**H**EKEIAAFESEIAAFESELQAYKGKG-NPEVEALRKEAAAIRDEAAAIRDE**H**QAYRLNGSG**A/C**
GRα_3D H_2DH	MGSWAEFKQRLAAIKTRLAAIK**S**R**HD**ALGGS-EAE**H**AA**D**EKEIAAFESEIAAFESELQAYKGKG-NPEVEALRKEAAAIRDEAAAIRDE**H**QAYRLNGSG**A/C**
GRα_3D H_3D	MGSWAEFKQRLAAIKTRLAAIK**S**R**HD**ALGGS-EAE**D**AA**H**EKEIAAFESEIAAFESELQAYKGKG-NPEVEALRKEAAAIRDEAAAIRDE**H**QAYRLNGSG**A/C**

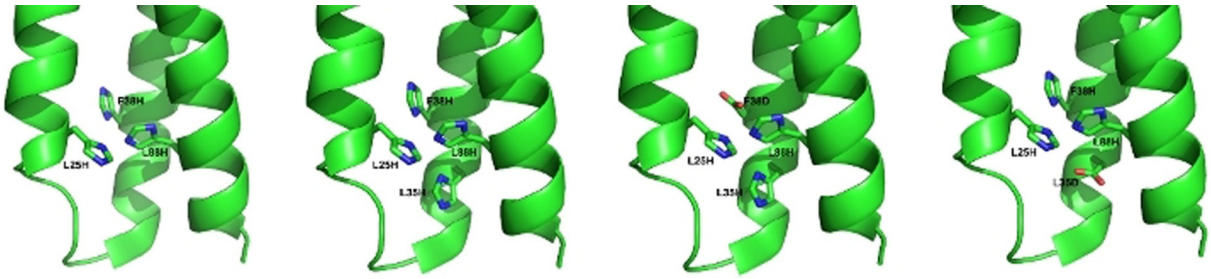

Figure 1. PyMol models of the designed His_3 (H_3), His_4 (H_4), His_2AspHis (H_2DH), and His_3Asp (H_3D) active sites within GRα_3D based on the crystal structure of GRα_3D (PDB: 6DS9).

tidines that replace leucine or phenylalanine (L25H, F38H, L88H) in positions analogous to the carbonic anhydrase mimic α_3D**H$_3$**, which also models the Cu^{I}-binding site of Cu-only SODs.[47] GRα_3D H$_4$ contains a fourth histidine in position 35 (L35H) to mimic the Cu^{II}-binding site of Cu-only SODs.[6,7] Constructs in which the fourth His residue was substituted by an Asp were created to test the effects of modulating the reduction potential of the bound Cu. To this end, GRα_3D H$_2$DH and GRα_3D H$_3$D, in which the Asp is either positioned in the same plane as two other His (L38D), or below a plane constituted by the three His (L35D), respectively, were designed. These constructs also model the active site of Fe/MnSODs, providing interesting insight into the selectivity and catalytic efficiency of substituting copper into this system.

Thermal stability of the apo- and Cu^{II} proteins

CD spectra of the apoproteins were obtained to test whether GRα_3D could properly fold with four large hydrophilic metal-binding residues mutated into the hydrophobic core (Figure S1 in the Supporting Information). The double minima bands at $\lambda = 208$ and 222 nm are representative for an α-helical secondary structure and indicate a well-folded three-helical bundle peptide.[57,58] We next sought to compare the destabilization effects of the differing active sites. Thermal denaturation of apo- and Cu^{II} proteins were studied and compared to that of GRα_3D by following the ellipticity of the proteins at $\lambda = 222$ nm at varying temperatures. The midpoint of unfolding (T_M) was determined by fitting the data to a two-state unfolding model by using the program CDpal.[58–60] These values are summarized in Table 3.

GRα_3D is structurally stable in the temperature range used with a melting temperature above 95 °C, which precludes calculating the aforementioned thermodynamic parameters. Three of the four constructs reported within this study, however, have melting temperatures below 95 °C, allowing for their direct measurement. Comparing these four constructs, we find that addition of a fourth residue destabilizes the protein as the T_M decreases over 10 °C between GRα_3D H$_3$ ($T_M > 95$ °C), and GRα_3D H$_2$DH, H$_3$D, and H$_4$ ($T_M \approx 80$ °C). Cu^{II}-bound peptide is thermodynamically more stable than the apopeptide, with T_M increasing by 5 to 10 °C depending on the construct. Overall, the data assess that the apoproteins and the Cu^{II} complexes are well folded at room temperature.

Interestingly, GRα_3D H$_4$ shows two steps in the unfolding process in both the apo- and Cu^{II}-bound form (Figure 2). The

Table 3. Thermodynamic parameters of unfolding for apo- and Cu^{II}-GRα_3D three-helix bundles determined by thermal denaturation.

Peptide	Apo peptide T_M [°C]	Cu peptide T_M [°C]
GRα_3D	> 95	–
GRα_3D H$_2$DH	79.8 ± 0.7	85.1 ± 0.9
GRα_3D H$_3$D	80.6 ± 0.6	88 ± 6
GRα_3D H$_3$	> 95	> 95
GRα_3D H$_4$	83.21 ± 0.01	93.8 ± 0.5

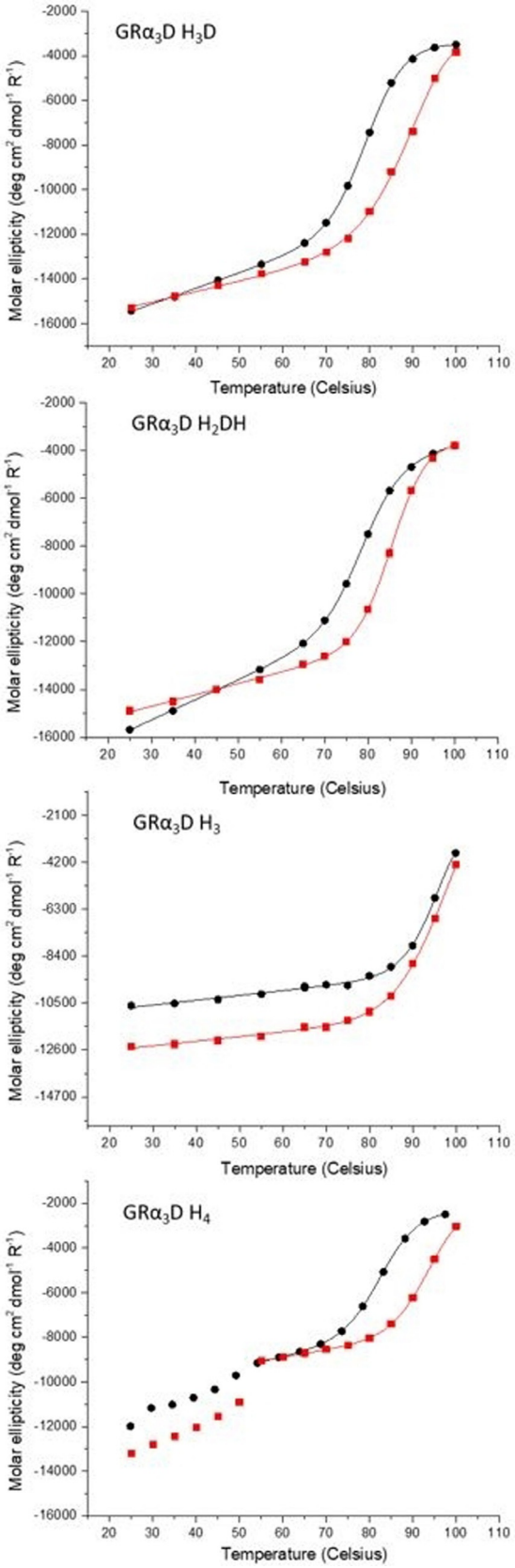

Figure 2. Thermal denaturation circular dichroism fits of GRα_3D H$_3$D, H$_2$DH, H$_3$, and H$_4$ (top to bottom). The spectra of the apoproteins are shown with black circles and the ones of the Cu^{II}-bound species with red squares. Only the second denaturation step was fit for GRα_3D H$_4$.

first transition to an intermediate state occurs at 55 °C. The second step occurs between 70 and 90 °C, similar to the other constructs. Upon cooling, the first state is no longer observed and reheating a sample results in a similar denaturation profile to the renaturation profile (Figure S2 in the Supporting Information).

Cu^{II} protein XAS and EPR characterization

X-ray absorption spectroscopy (XAS), consisting of both X-ray absorption near-edge structure (XANES) and extended X-ray absorption fine-structure (EXAFS), was done on Cu^{II}-GRα_3D H_3, Cu^{II}-GRα_3D H_4, Cu^{II}-GRα_3D H_2DH, and Cu^{II}-GRα_3D H_3D and analyzed to investigate the structural differences between these four SOD mimics (Figure 3). The average nearest-neighbor bond lengths was between 1.94 and 1.95 Å for all constructs analyzed, consistent with 4-coordinate N- or O-bound Cu^{II} (Table 4).

All constructs exhibit long distance backscatterers, which best fit to three His ligands. All fits attempted are included within the Supporting Information. This apparent similarity between the structure of the four constructs also extended to XANES analysis, where the 1s→3d transitions (peak at 8979 eV) for all four constructs were of similar height indicating an equivalent degree of tetrahedral character to their geometry.[61,62]

EPR spectra of the Cu^{II} proteins were collected in 50 mM 4-(2-hydroxyethyl)-1-piperazineethanesulfonic acid (HEPES) buffer, pH 7.5 at 100 K with a 2:1 protein/Cu^{II} ratio to ensure that all copper is bound (Figure 4). The *g* values and hyperfine

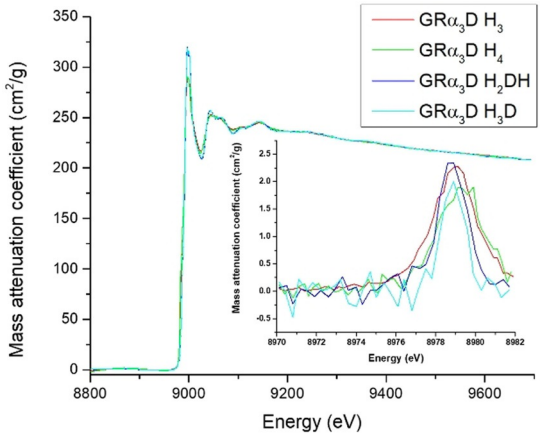

Figure 3. 1s→3d region of the Cu^{II} protein XANES spectra at pH 7.5 for every construct reported.

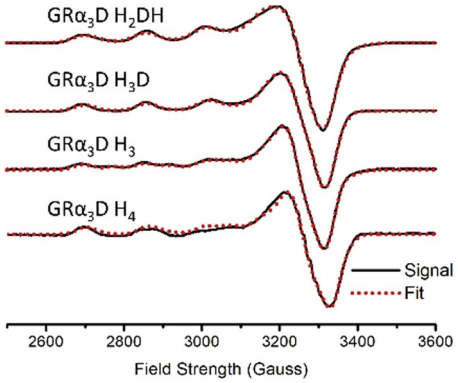

Figure 4. Electronparamagnetic resonance spectra of the constructs presented in this study recorded at pH 7.5. Fits were done by using the program SpinCount.

coupling constants of the Cu^{II} complexes were determined by fitting with the SpinCount software and are listed in Table 5.[63] Each complex has anisotropic *g* values with $g_x g_y < g_z$ characteristic of a $d_{x^2-y^2}$ single-occupied molecular orbital (SOMO).[64] Together with the EXAFS data, the results suggest 4-coordinate copper complexes in a distorted square-planar geometry.[64] Two distinct species (A and B in Table 5) are observed in the EPR spectra of Cu^{II}-GRα_3D H_3 and Cu^{II}-GRα_3D H_4. Simulation of the EPR spectrum of GRα_3D H_3 shows that form A is dominant and accounts for 75% of the signal observed, whereas form B accounts for 25%. For GRα3D H4 the two species are present in the same ratio. The EPR parameters of a Cu-only SOD found

Table 5. EPR parameters obtained from simulation of EPR spectra of Cu^{II} protein solutions.

		g_x	g_y	g_z	$A_{\|\|}$ [10^{-4} cm^{-1}]	$f = g_z/A_{\|\|}$ [cm]
GRα_3D H_3[a]	75% A	2.05	2.04	2.27	166	136.8
	25% B	2.05	2.03	2.22	149	149.0
GRα_3D H_4[a]	50% A	2.012	2.04	2.26	158	143.0
	50% B	2.04	2.03	2.23	188	119.6
GRα_3D H_2DH[a]	N/A	2.06	2.03	2.27	162	140.2
GRα_3D H_3D[a]	N/A	2.04	2.04	2.26	168	134.5
Cu only SOD[b]	N/A	2.05	2.05	2.26	≈140	161.4
Cu-(Fe) SOD[c]	N/A	2.05	2.05	2.37	136	174.3

[a] X-band EPR spectra recorded at 100 K on solutions of 1 mM $CuCl_2$ and 2 mM protein in 50 mM HEPES buffer containing 30% glycerol at pH 7.5, 9.3 GHz, 20.5 mW, 1 G. [b] Reference [7]. X-band EPR spectra of a Cu-only SOD from *Mycobacterium tuberculosis*. [c] Reference [70]. X-band EPR spectra recorded at 10 K of a copper-substituted Fe SOD from the archaeon *Acidianus ambivalens* in Tris/HCl buffer at pH 7, 9.6452 GHz, 20 mW, and 10.0 G.

Table 4. Cu^{II} EXAFS and XANES fitting parameters at pH 7.5.

Construct	Model	Cu–O/N* *R* [Å]	Cu–O/N* σ^2 [10^{-3} Å^2]	Cu–imid *R* [Å]	Cu–imid σ^2 [10^{-3} Å^2]	Avg. bond length [Å]	1s→3d area
GRα_3D H_3	His_3O_1	1.966	5.7	1.935	13.28	1.943	8.27
GRα_3D H_4	His_3N_1	1.881	4.4	1.972	6.23	1.949	6.89
GRα_3D H_2DH	His_3O_1	1.981	1.5	1.933	8.06	1.945	5.41
GRα_3D H_3D	His_3O_1	1.989	2.0	1.933	7.86	1.947	3.09

in *Mycobacterium tuberculosis* (His4 active site) and a copper-substituted FeSOD from the archaeon *Acidianus ambivalens* (His2AspHis) are given in Table 5.[7,65] The Cu^{II}-GR 3D derivatives have *g* values similar to these native enzymes and slightly higher $A_{||}$ values.

One may also attempt to correlate the hyperfine coupling constant observed in EPR to variation in activity between the constructs reported. The empirical factor $f = g_z/A_{||}$ correlates with tetrahedral distortions where values between 105 to 135 cm are indicative of square-planar geometry and higher values indicate distortion towards tetrahedral structures.[66,67] According to the values in Table 5, our constructs are more tetragonal than the native examples, which may be correlated to the decreased activity compared to the native enzymes. This is bolstered by the case of GRα_3D H_4 in which two species are evident at a 1:1 ratio. The GRα_3D H_4 species B has an *f* factor of 119.6 cm, indicating that this species is more tetragonal than GRα_3D H_4 species A with an *f* factor of 143.0 cm or any other construct reported in this manuscript. The activity of GRα_3D H_4 is also about half that of any of the other de novo constructs, which could be explained by species B being an inactive form. However, the differences in activity observed are too minor to make definitive claims about the requirement of tetrahedral distortion for the activity of CuSODs. Future studies with other designed proteins may allow to elucidate this relationship more clearly.

Cu^{I} protein XANES characterization

The XANES region of all four constructs were analyzed to investigate the coordination geometry. The Cu^{I} 1s→4p transition at 8982–8985 eV was analyzed to determine geometry differences between the constructs. The intensity of this peak is indicative of the coordination number with higher peak intensities correlating with lower coordination number.[68] GRα_3D H_3D has the lowest 1s→4p transition signal, indicative of a higher coordination number (Figure 5). GRα_3D H_3 and GRα_3D H_4 have similar intermediate transition signals. GRα_3D H_2DH has the highest transition signal, indicative of a lower coordination number, likely more 2-coordinate than 3-coordinate.

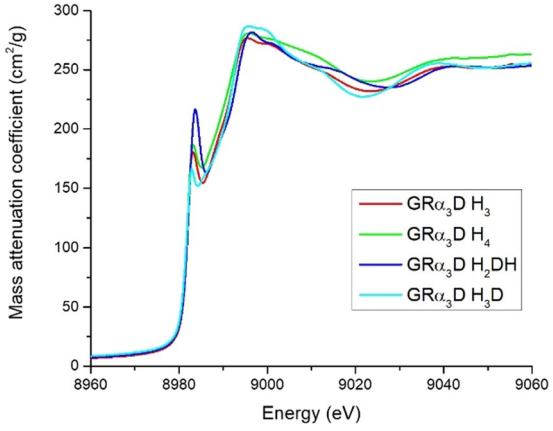

Figure 5. 1s→4p region of the Cu^{I} protein XANES spectra at pH 7.5 for every construct reported.

Reduction potentials, affinity, and SOD activity

The apparent standard potentials of Cu^{II} complexes containing a C-terminal Cys (Ala98Cys) and grafted on a gold electrode are listed in Table 6 with the cyclic voltammograms given in Figure S3 in the Supporting Information. All four constructs share á similar first-coordination sphere His_3N/O around the metal center as demonstrated by EXAFS analysis, however, the potential of GRα_3D H_3 is notably higher than that of the other three at 550 mV versus NHE compared to 420–470 mV versus NHE. The reduction potentials of the four constructs lie in between the potentials for oxidation of superoxide to peroxide (−0.18 V vs. NHE) and the reduction of superoxide to dioxygen (+0.91 V vs. NHE), which should enable catalysis of superoxide dismutation.

Table 6. Apparent standard potentials at pH 7.5, affinity constants, and SOD activity of the Cu^{II}–protein complexes.

	$E_{1/2}$[a] [mV vs. NHE]	Cu^{II} K_d [10^{-10} M]	Cu^{I} K_d [10^{-16} M]	IC_{50}[b] [μM]	k_{McF}[b] [10^6 $M^{-1}s^{-1}$]
GRα_3D H_3	550 ± 10	5.00 ± 0.17	1.22 ± 0.04	2.9 ± 0.6	3.0 ± 0.6
GRα_3D H_4	463 ± 10	5.7 ± 0.3	41 ± 2	8.0 ± 1.7	1.1 ± 0.2
GRα_3D H_2DH	420 ± 10	1.4 ± 0.4	54 ± 15	3.5 ± 1.1	2.6 ± 0.8
GRα_3D H_3D	470 ± 10	1.6 ± 0.2	8.8 ± 1.1	3.3 ± 0.3	2.6 ± 0.2

[a] The Cu^{II} proteins bearing a GSGC tail were grafted on an Au electrode and CV spectra were recorded at $v = 0.05\ V\,s^{-1}$ in an electrochemical working cell containing 50 mM HEPES buffer, pH 7.5 at room temperature. Counter electrode (CE): Pt wire, reference electrode: standard calomel electrode (SCE). [b] IC_{50} (μM) and k_{McF} (10^6 M^{-1s-1}) values were determined from triplicate experiments with Cu^{II} proteins (4:1 ligand/metal (L/M)) in 50 mM HEPES buffer, pH 7.5 with 100 μM XTT, 200 μM xanthine, and xanthine oxidase at 25 °C. $k_{XTT} = 8.6\ 10^4\ M^{-1s-1}$ (in phosphate-buffered saline (PBS) 50 mM, pH 7.8). Note that the rate reported for GRα_3D H_3 is a composite of two species as observed by EPR spectroscopy.

The Cu^{II} affinities for each of these four constructs were determined in an effort to account for these differences in the reduction potential (Table 6). Interestingly, though GRα_3D H_3 has a much higher reduction potential, it does not have a Cu^{II} affinity that is significantly different from that of GRα_3D H_2DH and GRα_3D H_3D. GRα_3D H_4 has the weakest Cu^{II} affinity with a K_d of 5.7×10^{-10} M, indicating that a fourth His residue does not play a significant role in the binding of Cu^{II}.

The calculated Cu^{I} affinities vary by two orders of magnitude across the four constructs. Cu^{I} binds tightest to GRα_3D H_3, with a K_d of 1.22×10^{-16} M GRα_3D H_3D has an intermediate Cu^{I} affinity (8.8×10^{-16} M), whereas both GRα_3D H_4 and H_2DH have a weaker affinity of 4.1×10^{-15} and 5.4×10^{-15} M, respectively (Table 6). Thus, adding a fourth peptide ligand decreases the Cu^{I} affinity of the protein but to different extents.

The SOD activities of the Cu proteins were measured by the McCord–Fridovich (McF) assay,[54,55] in which a secondary probe, sodium 2,3-bis-(2-methoxy-4-nitro-5-sulfophenyl)-2*H*-tetrazolium-5-carboxanilide (XTT), is used to determine the amount of superoxide removed from solution by the SOD mimic.[56] This assay is an indirect method to measure k_{cat}, but its reliability has been validated by direct methods (stopped-

flow and pulse radiolysis).[69–73] The assay was performed by using an excess of ligand (4:1 protein/Cu^{II}) to ensure no free copper is present. The IC_{50} is the concentration of SOD mimics at which 50% of the superoxide produced are dismutated by the SOD mimics. From this value, the k_{McF}, which can be compared to a catalytic rate constant, is calculated (Table 6).[2,54,55,69–72] GRα_3D H_3, GRα_3D H_2DH, and GRα_3D H_3D have similar IC_{50} (2.9–3.5 μM) and k_{McF} ($3\,10^6\,M^{-1}s^{-1}$) values, whereas GRα_3D H_4 has a lower SOD activity with the highest IC_{50} (8.0 μM) and lowest k_{McF} ($1.1\,10^6\,M^{-1}s^{-1}$). The apoproteins showed no SOD activity in the same concentration range. Additional controls were performed to check that no reaction occurs between the complex and formazan, and that the complex did not inhibit xanthine oxidase.

Discussion

The Cu-only SOD models presented here demonstrate that an exact reproduction of the active site is not necessary for modest SOD activity, but that the native residues play an important role in mediating this activity. Previous work with Cu/Zn SODs has shown that loss of even a single histidine in the active site results in a loss of SOD activity, typically through a loss of copper binding.[74–76] Although similar work on Cu-only SODs has not been performed, the present work suggests that all four histidine residues are not necessary for copper binding or SOD activity.

Studies of the Cu^{II}-bound forms indicate that all four models are structurally similar to Cu-only SODs. EPR experiments show that all four constructs are similar to both Cu^{II}-bound Cu-only SODs and Cu^{II}-substituted FeSODs.[7,65] The fourth protein ligand is not vital in modulating the structure of the Cu^{II}-binding environment as observed by EPR spectroscopy but does determine how many species are present in solution. Both constructs with an Asp ligand contain a single species, whereas a fourth His ligand or lack of a fourth protein ligand results in two species. This is confirmed by CD for GRα_3D H_4 as two unfolding steps are observed. Of these two species, only the more stable is observed upon cooling the sample. The fourth ligand, therefore, is necessary to restrict Cu^{II} binding to only a single confirmation. A fourth aspartate ligand, regardless of the position, may both coordinate the copper and orient a histidine residue in a single geometry. In both Cu/Zn and Cu-only SODs, an aspartate ligand orients the histidine residue that is bound only in the Cu^{II} form and loss of this residue results in a decrease of the SOD activity.[10,77] The second species present may simply be a result of different histidine coordination in these systems.

This is corroborated by the XAS data. Although these experiments cannot distinguish between multiple coordination states, the average indicates that all three histidines are bound in all four constructs. The fourth residue is likely an additional histidine in GRα_3D H_4 or an oxygen in the remaining three constructs. This oxygen may be from either the Asp ligand that is present in GRα_3D H_3D or H_2DH or a solvent residue. Thus, the Asp may be binding the copper as a fourth residue or the Cu^{II} coordination sphere is completed by water and the Asp solely acts to orient a histidine residue.

The Cu^{II} affinity is also affected by this fourth ligand. GRα_3D H_4 has the weakest Cu^{II} affinity, though only slightly weaker than GRα_3D H_3. If, however, the fourth ligand is an Asp residue instead, the Cu^{II} affinity increases by a factor of three. The position of this Asp residue does not have a significant effect on the affinity of the cupric ion. This indicates that a fourth oxygen ligand lends to tighter Cu^{II} binding than an imidazole ligand.

The fourth ligand is also important in modulating the copper reduction potential. Though all four constructs are catalytically active, GRα_3D H_3 has a much higher reduction potential than the constructs with a fourth amino acid ligand. Simply adding a fourth ligand decreases the midpoint potential by 80–130 mV, depending on the construct. This may be by removing solvent from the active site or by limiting the amount of rearrangement necessary to convert between the Cu^{I}- and Cu^{II}-bound forms.[78] None of the constructs is close to the desired 360 mV versus NHE, the midpoint between the reduction and oxidation of superoxide.[2,3] Disrupting the His_3 plane decreases the reduction potential by 50 mV from approximately 470 to 420 mV versus NHE, even though the Cu^{II} affinity remains unchanged between GRα_3D H_3D and H_2DH. The rearrangement of the Asp residue does more to stabilize the Cu^{II}-bound enzyme outside of increasing the affinity for Cu^{II}. The axial His in GRα_3D H_2DH is positioned in a more open, solvent-exposed cavity, which may allow for easier conversion between the Cu^{I} and Cu^{II} forms than in GRα_3D H_3D. In that construct the three histidines are located in a more spatially confined position within the peptide preventing such easy rearrangement.

Calculated Cu^{I} affinities also provide insight into the copper-binding environment. Unsurprisingly given the relatively weak Cu^{II} affinity and high reduction potential, GRα_3D H_3 has the tightest Cu^{I} affinity. GRα_3D H_2DH has the weakest Cu^{I} affinity, correlated with the low reduction potential and has the most two-coordinate character measured by XANES. Again, the identity and placement of the fourth ligand significantly affects cuprous binding. The identity of the axial ligand may account for this difference. With no axial peptide ligand (GRα_3D H_3), Cu^{I} binds with the highest affinity. In the Cu^{II}-bound form, the coordination sphere is completed with an axial solvent residue. This is most similar to GRα_3D H_3D, containing an axial Asp residue in addition to the His_3 plane, which results in an 8-fold loss in the Cu^{I} affinity. Maintaining the His_3 plane and adding an axial His residue (GRα_3D H_4) further decreases the Cu^{I} affinity (40× weaker than GRα_3D H_3). Disruption of the His_3 plane results in the greatest loss of Cu^{I} affinity and corresponds to the lowest reduction potential and highest Cu^{II} affinity. Clearly, GRα_3D H_2DH most favors the oxidized species.

All four constructs exhibit measurable SOD activity, though still three orders of magnitude slower than the native enzyme. They are more efficient than the previously reported manganese de novo mimic ($k_{McF} = 3.7\,10^5\,M^{-1}s^{-1}$), and have a similar activity to the iron SOD mimic reported by Benson et al. (k_{cat} $6.4\,10^6\,M^{-1}s^{-1}$).[43–45] The slowest construct, GRα_3D H_4, also has the weakest overall copper affinity, which is known to decrease

activity.[74–76] The remaining three constructs are 2.5–3-times faster but do not have statistically different rates. Thus, the trends in $Cu^{I/II}$ affinity and reduction potential do not correspond to trends in SOD activity. Previously, trends in reduction potential and SOD activity were observed for low-molecular-weight manganese SOD mimics, which show a better SOD activity when the reduction potential is closer to 0.36 V versus NHE, the midpoint potential between the oxidation and reduction of superoxide.[1–3,18,19,21] This observation applies for other copper SOD mimics.[1–3,18,19,20]

At this point, we are unable to determine if these peptides are rate-limited by product release or conversion between the oxidized and reduced metal species. There may be a measurable difference in substrate conversion among the three more active peptides following the reduction potential trend that is unobservable due to slow product release.

To conclude, this study is the first example of the design of functional Cu-only SOD mimics in de novo proteins and shows that all four His residues from the native active site are not required for SOD activity within a de novo construct. The activity of these constructs is much slower than that of the native enzyme and further studies will be done to address this. The Cu^{I} environment and dynamics between the Cu^{I}- and Cu^{II}-bound species will be characterized to provide insight into this difference. These states could provide insight into the rate of catalysis and may highlight the importance of the fourth copper ligand. By modifying this fourth ligand, both in ligand type and position, we aim to improve the rate of catalysis and determine the most efficient coordination environment for SOD activity in de novo protein models.

Experimental Section

Protein expression and purification: pET15B recombinant DNA plasmids (Celtek Genes) containing the gene for the GRα_3D constructs were transformed and expressed in *E. coli* BL21(DE3) competent cells (Life Technologies). The Ala98Cys derivatives of the GRα_3D constructs were prepared for electrochemical studies.

Colonies were inoculated in lysogeny broth (LB) medium (30 mL) and ampicillin (100 $\mu g\,mL^{-1}$) before being incubated at 37 °C and 175 rpm for 6–7 h. Autoinduction medium was inoculated with 10 mL/1 L culture flask at 25 °C and 250 rpm for 18 h to overexpress the proteins. Cells were pelleted, resuspended in 1.0 mM phosphate buffer saline solution containing 2 mM dithiothreitol and 2 mM ethylenediaminetetraacetic acid (EDTA) and lysed with a microfluidizer. The soluble protein was isolated after heat denaturation at 55 °C and acidification to pH 2 to remove contaminant proteins. The supernatant was filtered through a syringe (0.2 μm) and purified on a reversed-phase C18 HPLC by using a flow rate of 20 $mL\,min^{-1}$ and a linear gradient of 0.1% trifluoroacetic acid (TFA) in 3:7 CH_3CN/H_2O to 0.1% TFA in 7:3 CH_3CN/H_2O over 35 min. The molecular weight of the purified peptide was confirmed by ESI-MS (collected on a Micromass LCT Time-of-Flight Mass Spectrometer) and found to correspond to the expected protein mass after deletion of the N-terminal methionine residue. Protein concentrations were determined by measuring the absorbance with $\varepsilon_{280} = 8480\ M^{-1}\,cm^{-1}$.

Circular dichroism (CD) spectroscopy

CD spectra were collected on a Jasco J-1500 CD spectropolarimeter at 25 °C by using 1 cm path length quartz cuvettes. Samples contained 10 mM phosphate buffer, pH 7.0, and 10 μM protein. Cu^{II}-containing samples also included 11 μM $CuCl_2$. Thermal denaturation samples were heated at 5 °C min^{-1} and the ellipticity was recorded every 5 °C from 25 to 100 degrees after stabilization within ±0.1 °C of the desired temperature and an additional equilibration time of five minutes. Molar ellipticities ($[\theta]$) were calculated by using previously reported procedures.[58,79,80]

Cu^{II}-binding affinity

The binding affinity of Cu^{II} to each peptide was determined by using the competitive chelator 3,4-bis(oxamato)benzoic acid (baba). Solutions containing 50 μM peptide and 45 μM $CuCl_2$ in 50 mM HEPES pH 7.5 were titrated with 0.1 equivalents of baba with ten minutes of equilibration time between additions. The reverse titration was also performed with 50 μM baba and 45 μM $CuCl_2$ in 50 mM HEPES pH 7.5. The absorbance of the Cu^{II}–baba complex was monitored at $\lambda = 330$ nm and fit by using previously described methods.[81]

Cu^{I} binding affinity

The binding affinity of Cu^{I} was calculated at pH 7.5 based on the Cu^{II}-binding affinity and the reduction potentials of each peptide [Eq. 1]. A value of 0.159 V versus NHE was used for $E^{\circ}_{(Cu^{II/I},aq)}$.[82,83]

$$E^{\circ}_{Cu^{II/I}Pep} = E^{\circ}_{Cu^{II/I}aq} - \frac{2.303\ RT}{nF}\log\frac{K_{d_{Cu^{I}Pep}}}{K_{d_{Cu^{II}Pep}}} \quad (1)$$

Where $R = 8.314\ J\,mol^{-1}\,K^{-1}$, n = number of electrons, and $F = 9.648\times10^{4}\ C\,mol^{-1}$.

X-ray absorption spectroscopy

Cu^{II} samples were prepared with 1.0 mM Cu^{II} acetate and 1.5 mM peptide in 0 mM HEPES buffer at pH 7.5 in aerobic conditions. Samples were then lyophilized before transferring to sample cells as a dried powder. The Cu edge energy and 1s→4p transition of the Cu^{I} peptide were monitored and it was estimated that no more than 10% of the sample was photoreduced in the scans included in fits.

Cu^{I} samples were prepared with 1.0 mM tetrakis(acetonitrile)Cu^{I} hexafluorophosphate and 1.5 mM peptide in 50 mM HEPES buffer at pH 7.5 in anaerobic conditions. 50% glycerol were added to the solution as a glassing agent before sample solutions were loaded into an XAS sample cell and frozen in liquid nitrogen.

Measurements were carried out at Stanford Synchrotron Radiation Lightsource (SSRL) beamline 7-3 or 9-3 with a Si(220) double-crystal monochromator and a flat Rh-coated harmonic rejection mirror. Samples were maintained below 10 K with an Oxford Instruments liquid helium cryostat. Data were measured as fluorescence excitation spectra by using a 30- or 100-element Ge detector array (for beamlines 7-3 or 9-3, respectively) normalized to incident intensity measured with a N_2-filled ion chamber. Data were measured with steps of 0.25 eV in the XANES region (1 s integration time) and 0.05 $Å^{-1}$ in the EXAFS region to $k = 13.5\ Å^{-1}$ (1 ≈ 20 s integration, k^3-weighted). Energies were calibrated by assigning the lowest-energy inflection point of a copper metal foil as 8980.3 eV. An initial E_0 value of 9000 eV was used to convert data to k-space, and the background was removed by using a 3-region cubic spline.

EXAFS data were analyzed by using EXAFSPAK[84] and FEFF 9.0.[85] XANES data were normalized by using MBACK.[86] For analysis of the 1s→3d transitions, data were fitted with an arctan background with a pseudo-Voigt peak to model the rising edge and the 1s→3d peak, and this fitted background was then subtracted from the data. Cu^{I} spectra were analyzed in this way to determine the degree of oxidation of XAS samples. The absence of any peak above the noise in these spectra indicate that oxidation was minimal.

Single- and multiple-scattering fitting of EXAFS data were performed by using EXAFSPAK[84] with ab initio amplitude and phase parameters calculated by using FEFF 9.0.[85] An initial model of Cu–imidazole coordination was built based on the averaged bond lengths determined by single-scattering fitting of the EXAFS data. An initial model of Cu–imidazole coordination was built based on the average Cu–N bond lengths determined by single-scattering fitting of the EXAFS data, with the imidazole bond-lengths and angles taken as the average of all Cu–imidazole structures contained in the Cambridge Structural Database. All significant non-hydrogen paths, defined as those having an amplitude greater than 4% of the Cu–N amplitude, from this model were then loaded into EXAFSPAK and modeled as a rigid ligand. Initial estimates of the Debye–Waller factors for each Cu–imidazole shell were taken from calculations by Dimakis and Bunker.[87] The Cu–N bond length and Debye–Waller factor were allowed to vary, with the length and Debye–Waller factor for the other paths calculated based on the Cu–N values. Thus, the long distance scattering from the Cu–imid was modeled while only varying two independent variables.

Electron paramagnetic resonance (EPR) spectroscopy

X-band EPR spectra were collected on a Bruker EMX electron spin resonance spectrometer with a Varian liquid nitrogen cryostat at 100 K. EPR samples contained 1 mM $Cu^{II}Cl_2$, 1.5–2 mM peptide, 50 mM HEPES pH 7.4, and 30% glycerol. Each sample was flash-frozen in liquid N_2 before measurement. To obtain Cu^{II} EPR parameters, each spectrum was simulated on SpinCount.[63]

Electrochemistry

Cyclic voltammetry measurements were obtained on a Metrohm AUTOLAB potentiostat (PGSTAT302N).

The electrochemical apparatus contained a gold (Au) disk working electrode (1 mm diameter), a platinum wire counter electrode, and an aqueous saturated calomel electrode (SCE) as the reference electrode (0.241 V + SCE = normal hydrogen electrode). The gold surface was polished with diamond slurries having decreasing particle sizes in the following order: 6-3-1 μm. Au electrodes were conditioned in an electrochemical cell containing 0.5 M H_2SO_4, by scanning from −300 to +1500 mV vs. SCE at 500 mV s^{-1} until the cyclic voltammograms overlaid to indicate a homogeneous surface. After each electrode had been polished and conditioned, 50 μL of a 0.5 mM Cu^{II}–protein Ala98Cys solution in 50 mM HEPES buffer pH 7.5 were chemically adsorbed on the Au surface for 2–3 h. CVs were collected in 50 mM HEPES buffer, pH 7.5 at varying scan rates at room temperature (22–28 °C).

SOD activity

The SOD activity of the copper complexes was determined by using the indirect assay of McCord–Fridovich observing XTT reduction.[54–56] Superoxide anions were generated by a xanthine– oxidase system and detected by monitoring the formation of formazan at $\lambda = 470$ nm. The reactions were performed in 50 mM HEPES buffer pH 7.4 with 100 μM XTT and 200 μM xanthine. An appropriate amount of xanthine oxidase was added to start the reaction and generate a change in absorbance of 0.025–0.030 min^{-1}. The absorbance at $\lambda = 470$ nm was monitored for 1.5 min (slope $P1$) before addition of the SOD mimic, and for another 1.5 min after addition (slope $P2$). A plot of the ratio $(P1-P2)/P1$ as a function of SOD mimic concentration was used to calculate the inhibition concentration (IC_{50}) at which the reduction of XTT to formazan is inhibited by 50% ($P2 = {}^1/_2 P1$). A pseudo-catalytic rate constant, k_{McF}, was deduced from the IC_{50} value by using the relation: $k_{XTT} \times [XTT] = (k_{McF})(IC_{50})$, with $k_{XTT} = 5.94 \times 10^4$ $M^{-1} s^{-1}$ (pH 7.8).[2] In order to ensure that no free copper was present in solution the experiments were performed with an excess of protein (4:1 protein/metal). The measurements were performed in triplicate for each compound. Controls with the apoproteins showed no SOD activity. Controls were performed to determine that no inhibition of the xanthine–xanthine oxidase system resulted from the addition of the peptides. The rate of conversion of xanthine to urate was monitored at $\lambda = 290$ nm in the presence and absence of peptide and no inhibition was observed. Possible formazan complexation was monitored at $\lambda = 490$ nm after addition of peptide and no decrease in absorbance was detected, indicating no inhibition.[73,88,89]

Acknowledgements

V.P., K.K., and A.T. thank NIH grant R01 ES012236 for funding and A.T additionally acknowledges the Chateabriand Fellowship for funding. C.P. and E.M. acknowledge the network FrenchBIC (http://frenchbic.cnrs.fr/) for E.M.'s fellowship for her stay at Michigan. They also wish to thank ANR (ANR-15-CE07-0027) and Fondation pour la recherche médicale (DIE20151234413) for funding. O.I. acknowledges the financial support from Fundação para a Ciência e a Tecnologia [PTDC/QUI-BIQ/098406/2008) and the Marie Curie Actions (FP7-PEOPLE-IRG-230896).

Conflict of interest

The authors declare no conflict of interest.

Keywords: bioinorganic chemistry · enzymes · metalloenzymes · metalloproteins · protein design

[1] Y. Sheng, I. A. Abreu, D. E. Cabelli, M. J. Maroney, A.-F. Miller, M. Teixeira, J. S. Valentine, *Chem. Rev.* **2014**, *114*, 3854–3918.
[2] C. Policar in *Redox Active Therapeutics* (Eds.: J. S. Reboucas, I. Batinic-Haberle, I. Spasojevic, D. S. Warner, D. St. Clair), Springer, Cham, **2016**, pp. 125–164.
[3] I. A. Abreu, D. E. Cabelli, *Biochim. Biophys. Acta Proteins Proteomics* **2010**, *1804*, 263–274.
[4] J. D. Aguirre, V. C. Culotta, *J. Biol. Chem.* **2012**, *287*, 13541–13548.
[5] D. P. Barondeau, C. J. Kassmann, C. K. Bruns, J. A. Tainer, E. D. Getzoff, *Biochemistry* **2004**, *43*, 8038–8047.
[6] J. E. Gleason, A. Galaleldeen, R. L. Peterson, A. B. Taylor, S. P. Holloway, J. Waninger-Saroni, B. P. Cormack, D. E. Cabelli, P. J. Hart, V. C. Culotta, *Proc. Natl. Acad. Sci. USA* **2014**, *111*, 5866–5871.
[7] L. Spagnolo, I. Törö, M. D'Orazio, P. O'Neill, J. Z. Pedersen, O. Carugo, G. Rotilio, A. Battistoni, K. Djinović-Carugo, *J. Biol. Chem.* **2004**, *279*, 33447–33455.

[8] C. X. Li, J. E. Gleason, S. X. Zhang, V. M. Bruno, B. P. Cormack, V. C. Culotta, *Proc. Natl. Acad. Sci. USA* **2015**, *112*, E5336 – E5342.
[9] N. G. Robinett, R. L. Peterson, V. C. Culotta, *J. Biol. Chem.* **2018**, *293*, 4636 – 4643.
[10] R. L. Peterson, A. Galaleldeen, J. Villarreal, A. B. Taylor, D. E. Cabelli, P. J. Hart, V. C. Culotta, *J. Biol. Chem.* **2016**, *291*, 20911 – 20923.
[11] H. J. Forman, I. Fridovich, *Arch. Biochem. Biophys.* **1973**, *158*, 396 – 400.
[12] S. B. Choudhury, J.-W. Lee, G. Davidson, Y.-I. Yim, K. Bose, M. L. Sharma, S.-O. Kang, D. E. Cabelli, M. J. Maroney, *Biochemistry* **1999**, *38*, 3744 – 3752.
[13] Y.-H. Zhou, H. Fu, W.-X. Zhao, W.-L. Chen, C.-Y. Su, H. Sun, L.-N. Ji, Z.-W. Mao, *Inorg. Chem.* **2007**, *46*, 734 – 739.
[14] D. Árus, A. Jancsó, D. Szunyogh, F. Matyuska, N. V. Nagy, E. Hoffmann, T. Körtvélyesi, T. Gajda, *J. Inorg. Biochem.* **2012**, *106*, 10 – 18.
[15] D. P. Riley, *Chem. Rev.* **1999**, *99*, 2573 – 2588.
[16] D. Salvemini, C. Muscoli, D. P. Riley, S. Cuzzocrea, *Pulm. Pharmacol. Ther.* **2002**, *15*, 439 – 447.
[17] O. Iranzo, *Bioorg. Chem.* **2011**, *39*, 73 – 87.
[18] I. Batinic-Haberle, A. Tovmasyan, E. R. Roberts, Z. Vujaskovic, K. W. Leong, I. Spasojevic, *Antioxid. Redox Signaling* **2014**, *20*, 2372 – 2415.
[19] I. Batinić-Haberle, J. S. Rebouças, I. Spasojević, *Antioxid. Redox Signaling* **2010**, *13*, 877 – 918.
[20] R. P. Bonomo, G. Impellizzeri, D. La Mendola, G. Maccarrone, G. Pappalardo, A. Santoro, G. Tabbi, G. Vecchio, E. Rizzarelli in *Metal – Ligand Interactions: Molecular, Nano-, Micro- and Macro-systems in Complex Environments*, (Eds.: N. Russo, D. R. Salahub, M. Witko), Kluwer Academic Publishers, Dordrecht, **2003**, pp. 41 – 63.
[21] I. Batinic-Haberle, A. Tovmasyan, I. Spasojevic, *Antioxid. Redox Signaling* **2018**, *29*, 1691 – 1724.
[22] I. Batinic-Haberle, M. E. Tome, *Redox Biol* **2019**, *25*, 101139.
[23] J.-J. Zhang, Q.-H. Luo, D.-L. Long, J.-T. Chen, F.-M. Li, A.-D. Liu, *J. Chem. Soc. Dalton Trans.* **2000**, 1893 – 1900.
[24] C.-J. Feng, Q.-H. Luo, Z.-L. Wang, M.-C. Shen, H.-W. Wang, M.-H. Zhao, *J. Inorg. Biochem.* **1999**, *75*, 1 – 6.
[25] A. Kotynia, T. Janek, Ż. Czyżnikowska, S. Bielińska, W. Kamysz, J. Brasuń, *Int. J. Pept. Res. Ther.* **2017**, *23*, 431 – 439.
[26] G. Csire, S. Timári, J. Asztalos, J. M. Király, M. Kiss, K. Várnagy, *J. Inorg. Biochem.* **2017**, *177*, 198 – 210.
[27] S. Timári, R. Cerea, K. Várnagy, *J. Inorg. Biochem.* **2011**, *105*, 1009 – 1017.
[28] I. N. Jakab, O. Lőrincz, A. Jancsó, T. Gajda, B. Gyurcsik, *Dalton Trans.* **2008**, 6987.
[29] A. Jancsó, Z. Paksi, N. Jakab, B. Gyurcsik, A. Rockenbauer, T. Gajda, *Dalton Trans.* **2005**, 3187.
[30] B. Bóka, A. Myari, I. Sóvágó, N. Hadjiliadis, *J. Inorg. Biochem.* **2004**, *98*, 113 – 122.
[31] L. L. Costanzo, G. D. Guidi, S. Giuftida, E. Rizzarelli, G. Vecchio, *J. Inorg. Biochem.* **1993**, *50*, 273 – 281.
[32] S. Kubota, J. T. Yang, *Proc. Natl. Acad. Sci. USA* **1984**, *81*, 3283 – 3286.
[33] R. Brigelius, R. Spöttl, W. Bors, E. Lengfelder, M. Saran, U. Weser, *FEBS Lett.* **1974**, *47*, 72 – 75.
[34] P.-S. Huang, S. E. Boyken, D. Baker, *Nature* **2016**, *537*, 320 – 327.
[35] J. W. Bryson, S. F. Betz, H. S. Lu, D. J. Suich, H. X. Zhou, K. T. O'Neil, W. F. DeGrado, *Science* **1995**, *270*, 935 – 941.
[36] J. W. Bryson, J. R. Desjarlais, T. M. Handel, W. F. Degrado, *Protein Sci.* **1998**, *7*, 1404 – 1414.
[37] W. F. DeGrado, C. M. Summa, V. Pavone, F. Nastri, A. Lombardi, *Annu. Rev. Biochem.* **1999**, *68*, 779 – 819.
[38] J. S. Plegaria, V. L. Pecoraro, *Isr. J. Chem.* **2015**, *55*, 85 – 95.
[39] M. Tegoni, *Eur. J. Inorg. Chem.* **2014**, 2177 – 2193.
[40] D. Ghosh, V. L. Pecoraro, *Curr. Opin. Chem. Biol.* **2005**, *9*, 97 – 103.
[41] F. Yu, V. M. Cangelosi, M. L. Zastrow, M. Tegoni, J. S. Plegaria, A. G. Tebo, C. S. Mocny, L. Ruckthong, H. Qayyum, V. L. Pecoraro, *Chem. Rev.* **2014**, *114*, 3495 – 3578.
[42] M. L. Zastrow, V. L. Pecoraro, *Coord. Chem. Rev.* **2013**, *257*, 2565 – 2588.
[43] U. P. Singh, R. K. Singh, Y. Isogai, Y. Shiro, *Int. J. Pept. Res. Ther.* **2006**, *12*, 379 – 385.
[44] A. L. Pinto, H. W. Hellinga, J. P. Caradonna, *Proc. Natl. Acad. Sci. USA* **1997**, *94*, 5562 – 5567.
[45] D. E. Benson, M. S. Wisz, H. W. Hellinga, *Proc. Natl. Acad. Sci. USA* **2000**, *97*, 6292 – 6297.
[46] S. T. R. Walsh, H. Cheng, J. W. Bryson, H. Roder, W. F. DeGrado, *Proc. Natl. Acad. Sci. USA* **1999**, *96*, 5486 – 5491.
[47] V. M. Cangelosi, A. Deb, J. E. Penner-Hahn, V. L. Pecoraro, *Angew. Chem. Int. Ed.* **2014**, *53*, 7900 – 7903; *Angew. Chem.* **2014**, *126*, 8034 – 8037.
[48] J. S. Plegaria, M. Duca, C. Tard, T. J. Friedlander, A. Deb, J. E. Penner-Hahn, V. L. Pecoraro, *Inorg. Chem.* **2015**, *54*, 9470 – 9482.
[49] J. S. Plegaria, S. P. Dzul, E. R. P. Zuiderweg, T. L. Stemmler, V. L. Pecoraro, *Biochemistry* **2015**, *54*, 2858 – 2873.
[50] A. G. Tebo, A. Quaranta, C. Herrero, V. L. Pecoraro, A. Aukauloo, *ChemPhotoChem* **2017**, *1*, 89 – 92.
[51] A. G. Tebo, T. B. J. Pinter, R. Garcia-Serres, A. L. Speelman, C. Tard, O. Seneque, G. Blondin, J. M. Latour, J. Penner-Hahn, N. Lehnert, V. L. Pecoraro, *Biochemistry* **2018**, *57*, 2308 – 2316.
[52] K. J. Koebke, F. Yu, E. Salerno, C. Van Stappen, A. G. Tebo, J. E. Penner-Hahn, V. L. Pecoraro, *Angew. Chem. Int. Ed.* **2018**, *57*, 3954 – 3957; *Angew. Chem.* **2018**, *130*, 4018 – 4021.
[53] K. J. Koebke, L. Ruckthong, J. L. Meagher, E. Mathieu, J. Harland, A. Deb, N. Lehnert, C. Policar, C. Tard, J. E. Penner-Hahn, J. A. Stuckey, V. L. Pecoraro, *Inorg. Chem.* **2018**, *57*, 12291 – 12302.
[54] I. Fridovich, *J. Biol. Chem.* **1970**, *245*, 4053 – 4057.
[55] J. M. McCord, I. Fridovich, *J. Biol. Chem.* **1969**, *244*, 6049 – 6055.
[56] M. W. Sutherland, B. A. Learmonth, *Free Radical Res.* **1997**, *27*, 283 – 289.
[57] Y.-H. Chen, J. T. Yang, K. H. Chau, *Biochemistry* **1974**, *13*, 3350 – 3359.
[58] T. E. Creighton, *Protein structure: A practical approach*, Oxford University Press, New York, **1997**.
[59] N. J. Greenfield, *Nat. Protoc.* **2006**, *1*, 2527 – 2535.
[60] M. Niklasson, C. Andresen, S. Helander, M. G. Roth, A. Zimdahl Kahlin, M. Lindqvist Appell, L. G. Martensson, P. Lundstrom, *Protein Sci.* **2015**, *24*, 2055 – 2062.
[61] J. E. Hahn, R. A. Scott, K. O. Hodgson, S. Doniach, S. R. Desjardins, E. I. Solomon, *Chem. Phys. Lett.* **1982**, *88*, 595 – 598.
[62] F. de Groot, G. Vankó, P. Glatzel, *J. Phys. Condens. Matter* **2009**, *21*, 104207.
[63] A. P. Golombek, M. P. Hendrich, *J. Magn. Reson.* **2003**, *165*, 33 – 48.
[64] E. I. Solomon, D. E. Heppner, E. M. Johnston, J. W. Ginsbach, J. Cirera, M. Qayyum, M. T. Kieber-Emmons, C. H. Kjaergaard, R. G. Hadt, L. Tian, *Chem. Rev.* **2014**, *114*, 3659 – 3853.
[65] S. Kardinahl, S. Anemüller, G. Schäfer, *Biol. Chem.* **2000**, *381*, 1089 – 1101.
[66] U. Sakaguchi, A. W. Addison, *J. Chem. Soc. Dalton Trans.* **1979**, 600 – 608.
[67] A. Diaz, R. Pogni, R. Cao, R. Basosi, *Inorg. Chim. Acta* **1998**, *275 – 276*, 552 – 556.
[68] L. S. Kau, D. J. Spira-Solomon, J. E. Penner-Hahn, K. O. Hodgson, E. I. Solomon, *J. Am. Chem. Soc.* **1987**, *109*, 6433 – 6442.
[69] M. Eckshtain, I. Zilbermann, A. Mahammed, I. Saltsman, Z. Okun, E. Maimon, H. Cohen, D. Meyerstein, Z. Gross, *Dalton Trans.* **2009**, 7879 – 7882.
[70] I. Spasojevic, I. Batinic-Haberle, R. D. Stevens, P. Hambright, A. N. Thorpe, J. Grodkowski, P. Neta, I. Fridovich, *Inorg. Chem.* **2001**, *40*, 726 – 739.
[71] S. Durot, C. Policar, F. Cisnetti, F. Lambert, J.-P. Renault, G. Pelosi, G. Blain, H. Korri-Youssoufi, J.-P. Mahy, *Eur. J. Inorg. Chem.* **2005**, 3513 – 3523.
[72] S. Durot, F. Lambert, J.-P. Renault, C. Policar, *Eur. J. Inorg. Chem.* **2005**, 2789 – 2793.
[73] F. C. Friedel, D. Lieb, I. Ivanovic-Burmazovic, *J. Inorg. Biochem.* **2012**, *109*, 26 – 32.
[74] M. T. Carri, A. Battistonia, F. Polizio, A. Desideri, G. Rotilio, *FEBS Lett.* **1994**, *356*, 314 – 316.
[75] J. Wang, H. Slunt, V. Gonzales, D. Fromholt, M. Coonfield, N. G. Copeland, N. A. Jenkins, D. R. Borchelt, *Hum. Mol. Genet.* **2003**, *12*, 2753 – 2764.
[76] J. Wang, A. Caruano-Yzermans, A. Rodriguez, J. P. Scheurmann, H. H. Slunt, X. Cao, J. Gitlin, P. J. Hart, D. R. Borchelt, *J. Biol. Chem.* **2007**, *282*, 345 – 352.
[77] C. L. Fisher, D. E. Cabelli, J. A. Tainer, R. A. Hallewell, E. D. Getzoff, *Proteins Struct. Funct. Bioinf.* **1994**, *19*, 24 – 34.
[78] G. R. Moore, G. W. Pettigrew, N. K. Rogers, *Proc. Natl. Acad. Sci. USA* **1986**, *83*, 4998 – 4999.
[79] C. A. Rohl, R. L. Baldwin, *Biochemistry* **1997**, *36*, 8435 – 8442.
[80] P. Luo, R. L. Baldwin, *Biochemistry* **1997**, *36*, 8413 – 8421.

[81] A. Conte-Daban, V. Borghesani, S. Sayen, E. Guillon, Y. Journaux, G. Gontard, L. Lisnard, C. Hureau, *Anal. Chem.* **2017**, *89*, 2155 – 2162.
[82] M. Tegoni, F. Yu, M. Bersellini, J. E. Penner-Hahn, V. L. Pecoraro, *Proc. Natl. Acad. Sci. USA* **2012**, *109*, 1 – 6.
[83] P. Atkins, T. Overton, J. Rourke, M. Weller, F. Armstrong, M. Hagerman, *Inorganic Chemistry*, 5th ed., Freeman and Company, New York, **2010**.
[84] G. N. George, I. J. Pickering, EXAFSPAK, http://ssrl.slac.stanford.edu/≈george/exafspak/exafs.htm.
[85] A. L. Ankudinov, J. J. Rehr, *Phys. Rev. B* **1997**, *56*, R1712 – R1716.
[86] T.-C. Weng, G. S. Waldo, J. E. Penner-Hahn, *J. Synchrotron Radiat.* **2005**, *12*, 506 – 510.
[87] N. Dimakis, G. Bunker, *Phys. Rev. B* **2004**, *70*, 195114.
[88] K. M. Faulkner, S. I. Liochev, I. Fridovich, *J. Biol. Chem.* **1994**, *269*, 23471 – 23476.
[89] R. H. Weiss, A. G. Flickinger, W. J. Rivers, M. M. Hardy, K. W. Aston, U. S. Ryan, D. P. Riley, *J. Biol. Chem.* **1993**, *268*, 23049 – 23054.

Manuscript received: August 20, 2019
Revised manuscript received: October 4, 2019
Accepted manuscript online: November 11, 2019
Version of record online: December 3, 2019